Backbone Dynamics in Dihydrofolate Reductase Complexes: Role of Loop Flexibility in the Catalytic Mechanism†

Michael J. Osborne,‡,§ Jason Schnell,‡ Stephen J. Benkovic,|| H. Jane Dyson,‡ and Peter E. Wright*,‡

Department of Molecular Biology and Skaggs Institute for Chemical Biology, The Scripps Research Institute, 10550 North Torrey Pines Road, La Jolla, California 92037, and Department of Chemistry, Pennsylvania State University, State College, Pennsylvania

Received March 27, 2001; Revised Manuscript Received June 13, 2001

ABSTRACT: To elucidate the influence of local motion of the polypeptide chain on the catalytic mechanism of an enzyme, we have measured ^{15}N relaxation data for *Escherichia coli* dihydrofolate reductase in three different complexes, representing different stages in the catalytic cycle of the enzyme. NMR relaxation data were analyzed by the model-free approach, corrected for rotational anisotropy, to provide insights into the backbone dynamics. There are significant differences in the backbone dynamics in the different complexes. Complexes in which the cofactor binding site is occluded by the Met20 loop display large amplitude motions on the picosecond/nanosecond time scale for residues in the Met20 loop, the adjacent βF−βG loop and for residues 67−69 in the adenosine binding loop. Formation of the closed Met20 loop conformation in the ternary complex with folate and $NADP^+$, results in attenuation of the motions in the Met20 loop and the βF−βG loop but leads to increased flexibility in the adenosine binding loop. New fluctuations on a microsecond/millisecond time scale are observed in the closed E:folate:$NADP^+$ complex in regions that form hydrogen bonds between the Met20 and the βF−βG loops. The data provide insights into the changes in backbone dynamics during the catalytic cycle and point to an important role of the Met20 and βF−βG loops in controlling access to the active site. The high flexibility of these loops in the occluded conformation is expected to promote tetrahydrofolate-assisted product release and facilitate binding of the nicotinamide ring to form the Michaelis complex. The backbone fluctuations in the Met20 loop become attenuated once it closes over the active site, thereby stabilizing the nicotinamide ring in a geometry conducive to hydride transfer. Finally, the relaxation data provide evidence for long-range motional coupling between the adenosine binding loop and distant regions of the protein.

Dynamic processes are implicit in the catalytic function of all enzymes. Protein dynamics are implicated in events such as binding of substrate or cofactor, product release, and allosteric change. In addition, the catalyzed reaction itself involves an inherently dynamic process with changes in atom positions required along the reaction coordinate (*1*). Although there is considerable evidence both from theory and from experiment that many enzymes are inherently flexible, the fundamental question of how protein fluctuations couple to catalytic function remains unanswered. In contrast to reactions in solution, the enzymic environment is preorganized to be complementary to the transition state configuration of the reactants; the bound substrates in the Michaelis complex adopt conformations that closely resemble the transition state (the so-called near attack conformers or NACs; *2*). It is possible that protein motions couple to the formation of NACs and hence influence the probability of reaction. For example, for the enzyme dihydrofolate reductase (DHFR),[1] the chemical reaction occurs on the millisecond time scale, which is sufficient time for many conformational changes to occur that could potentiate the reaction. The reaction rate measured under pre-steady-state conditions (ca. 1000 s^{-1}) exhibits a deuterium isotope effect of 3, an indication that no kinetically significant reorganization of the Michaelis complex is necessary in the catalytic step (*3*).

Other motions of the protein can also contribute to the catalytic reaction. To achieve catalysis, enzymes frequently undergo conformational changes that involve functionally relevant surface loops that adopt an "open" configuration to allow access of the substrate and release of the product from the active site and a "closed" conformation, which protects the active site from the bulk solvent and facilitates favorable interactions necessary for catalysis (*1*). Studies by NMR (*4*−*7*), X-ray crystallography (*8*−*10*), and molecular dynamics simulations (*11*) have shown that motions on physiologically relevant time scales of functionally relevant loops in enzymes

† This work was supported by Grant GM 56879 from the National Institutes of Health.

* Corresponding author tel: (858) 784-9721; fax: (858) 784-9822; e-mail: wright@scripps.edu.

‡ The Scripps Research Institute.

§ Present address: Biotechnology Research Institute, National Research Council Canada, 6100 Royalmount Avenue, Montreal, Quebec H4P 2R2, Canada

|| Pennsylvania State University.

[1] Abbreviations: NMR, nuclear magnetic resonance; NOE, nuclear Overhauser effect; DHFR, dihydrofolate reductase; $NADP^+$, nicotinamide adenine dinucleotide phosphate; NADPH, reduced nicotinamide adenine dinucleotide phosphate; DHF, 7,8-dihydrofolate; THF, 5,6,7,8-tetrahydrofolate; DHNADPH, 5,6-dihydro NADPH; NOESY, nuclear Overhauser enhancement spectroscopy.

10.1021/bi010621k CCC: $20.00
Published on Web 07/25/2001

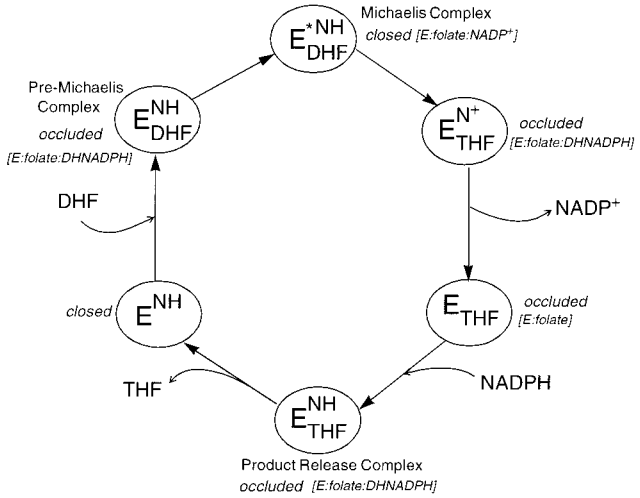

FIGURE 1: Reaction cycle of *E. coli* DHFR adapted from ref *17*. The complexes are as follows: E^{NH}_{DHF}, pre-Michaelis complex of dihydrofolate and NADPH; E^{*NH}_{DHF}, Michaelis complex of dihydrofolate and NADPH; E^{N+}_{THF}, product complex of tetrahydrofolate and $NADP^+$; E_{THF}, binary complex with tetrahydrofolate; E^{NH}_{THF}, ternary complex of tetrahydrofolate and NADPH; E^{NH}, binary complex with NADPH. The conformation of the Met20 loop, deduced from X-ray crystallographic (*10*) and NMR studies[2] is indicated for each complex. The model complexes studied in the present work are shown with the complexes of the reaction cycle that they most closely resemble.

are common. The importance of these motions, which have been termed temporal gating (*12*) or conformational gating (*13*), in enzyme catalysis is still not known, although various theories have been proposed (*1*, *11*, *13*−*16*). One may imagine that the closing of the active site through movement of loops may complete the formation of a Michaelis complex populated with an increased fraction of NACs.

Escherichia coli DHFR, which utilizes NADPH to reduce 7,8-dihydrofolate (DHF) to form the product 5,6,7,8-tetrahydrofolate (THF) (Figure 1), is uniquely suited for investigating the coupling between protein dynamics and catalytic function. The enzyme has been extensively studied: 3D structures of a large number of substrate, cofactor, and inhibitor complexes have been determined (see, e.g., ref *10*), and the kinetic mechanism has been thoroughly evaluated (*17*) for the wild-type enzyme and catalytically compromised mutants. To fully comprehend the significance of loop motions as well as other dynamical processes along the reaction coordinate that may couple to catalysis of the chemical step, information on the dynamics of all the intermediate states implicated along its reaction pathway (Figure 1) is required. X-ray structures of complexes of DHFR bound to cofactor and substrate analogues (ref *10* and references therein) show that the protein is formed from an essentially rigid scaffold comprising an eight-strand β-sheet flanked by four α-helices. Three distinct conformations were observed for a surface loop formed by residues 9−24 (termed the Met20 loop or loop 1), depending on the nature of the bound ligand; this led to the proposal (*10*) that interactions of this loop with other surface loops, namely, the loop between β-strands F and G (F−G loop, residues 116−132) and between β-strands G and H (G−H loop, residues 142−150), are important for catalysis.

[2] Unpublished data.

NMR data show that in the apo enzyme the Met20 loop fluctuates between two conformations at a rate comparable with THF dissociation (*6*), which is rate determining (*17*). Further NMR studies have shown that the binding of folate attenuates the low-frequency motions of the Met20 loop but does not abrogate all loop motion (*5*). High-frequency motions on the nanosecond/picosecond time scale persist in the peptide backbone for residues 16−19 of the Met20 loop as well as other regions of DHFR known to undergo ligand-dependent conformational change, including the F−G loop (*5*).

There is considerable evidence from site-directed mutagenesis implicating these flexible loops in DHFR function (*18*−*21*). Deletion of the central residues in the Met20 loop (achieved by replacement of residues Met16−Ala19 by a single glycine) results in a striking 500-fold decrease in the rate of hydride transfer (*18*). Moreover, substitution or deletion of mobile residues observed for the binary folate complex in the F−G loop (residues 121 and 122) significantly alter the kinetics of DHFR, even though these residues are ~19 Å away from the active site (*19*−*21*). In view of the X-ray analyses of Sawaya and Kraut (*10*), which suggest that loop interactions modulate ligand binding and turnover, the striking effects of F−G loop mutations on the kinetics are consistent with a role for loop dynamics in catalytic function. Extensive molecular dynamics simulations on three DHFR ternary complexes have shown that motions in the functionally relevant loops are sensitive to the nature of the ligand (*22*). Furthermore, correlated motions were observed in the Michaelis complex involving residues that have been implicated in catalysis but are not in the active site, providing further indications that dynamics could be important for catalysis.

In this paper, we compare backbone ^{15}N relaxation data for the following three complexes of DHFR: the binary complex with the substrate analogue folate (E:folate); the ternary complex with folate and an inactive cofactor analogue, 5,6-dihydroNADPH (E:folate:DHNADPH); and the ternary complex with folate and $NADP^+$ (E:folate:$NADP^+$). Following the arguments of Sawaya and Kraut (*10*) and for reasons given below, we propose that these complexes model the product binary complex (E:THF), both a pre-Michaelis complex (E:DHF:NADPH) and the product release complex (E:THF:NADPH), and the Michaelis complex (E*:DHF:NADPH), respectively (Figure 1). Our data show that the complexes have significantly different dynamic behavior at functionally relevant sites and, in conjunction with the available kinetic, structural, and mutagenesis results, strongly support a functional role for both nanosecond and millisecond/microsecond motions in the catalytic function of DHFR.

MATERIALS AND METHODS

Sample Preparation. Recombinant wild-type *E. coli* DHFR was overexpressed and purified as described previously (*21*, *23*). DHFR purity was checked by MALDI analysis. Pure DHFR was exchanged into the NMR buffer (0.1 M KCl, 1 mM EDTA, 1 mM [^{2}H]DTT, and 50 mM potassium phosphate, pH 6.8) using a NAP5 column. To prevent the potential degradation of cofactor and substrate, the NMR buffer was purged extensively with argon gas prior to use.

The DHFR concentration was determined spectrophotometrically using a molar extinction coefficient of 31 100 M^{-1} cm^{-1}. Details of sample preparation have been described elsewhere for the binary folate (E:folate) (*5*) and the ternary folate−DHNADPH (E:folate:DHNADPH) complexes (*23*). The concentration of the E:folate complex in the present experiments was 1.5 mM, and the folate concentration was a 6-fold excess. The E:folate:$NADP^+$ complex was prepared from fresh 0.1 M stock solutions of folate and $NADP^+$ (both purchased from Sigma) in NMR buffer. Addition of base was required to fully dissolve folic acid. Dissolution of $NADP^+$ caused a decrease in pH of the NMR buffer, which was corrected by immediate addition of NaOH to prevent acid hydrolysis of $NADP^+$. Aliquots of the stock folate and $NADP^+$ solutions were added to DHFR in approximately 6-fold excess. The final concentration of DHFR in the E:folate:$NADP^+$ complex was ~1.2 mM.

NMR Spectroscopy. Backbone ^1H, ^{15}N, and ^{13}C resonance assignments for E:folate:DHNADPH and E:folate:$NADP^+$ were made using triple-resonance methods.[2] Assignments for the E:folate complex have been reported previously (*24*). A 3D $^1H-^{15}N$ NOESY−HSQC spectrum of the E:folate:DHNADPH complex was recorded with a mixing time of 80 ms to determine the conformation of the Met20 loop. To investigate the orientation of the nicotinamide ring in the E:folate:DHNADPH complex by intermolecular NOEs, a select filter edit NMR experiment (*25*) was recorded on $^{15}N/^{13}C$-labeled DHFR in the presence of unlabeled folate and DHNADPH (further details of this experiment will be given elsewhere). ^{15}N T_1 and T_2 relaxation times and the $\{^1H\}-^{15}N$ NOE were measured at 306.4 K (calibrated with neat methanol or with ethylene glycol) for the ternary complexes, using a Bruker DRX spectrometer equipped with a triple-resonance probe and triple-axis pulsed field gradients operating at a ^1H Larmor frequency of 600.13 MHz. Heteronuclear NOE and T_2 data were also measured at 500 MHz for the E:folate:DHNADPH complex. All relaxation data were acquired with the pulse sequences described by Farrow et al. (*26*), using flip-back methods for water suppression and sensitivity enhancement and coherence selection via pulsed field gradients. Relaxation data have been reported previously for the E:folate complex at 303 K (*5*); however, for comparison with the ternary complexes, the model-free analysis for E:folate has been repeated with a new set of relaxation data, acquired for the purposes of this comparison using the gradient flip-back method for water suppression. A 1-ms interval between refocusing π pulses was used in the Carr−Purcell−Meiboom−Gill (CPMG) pulse train. Cross-correlation effects were suppressed during the CPMG pulse train by the application of ^1H π pulses synchronously with every second echo (*27*). Spectrometer settings for the data acquired for the two ternary complexes and for the binary folate complex are noted in the following discussion as ternary settings (binary settings). Spectra were acquired with 4096 (2048) complex points in t_2 and 256 (256) complex points in t_1. The ^1H and ^{15}N carriers were positioned on the water at 4.67 ppm (4.70) and at 118 ppm (114.7), respectively. Nitrogen chemical shifts were referenced indirectly using the $^1H-^{15}N$ ratio of 0.101 329 14 for TMS (*28*, *29*). Spectral widths were 16 ppm (16) for ^1H and 35 ppm (41) for ^{15}N. The R_1 and R_2 experiments were acquired with 16 (8) transients per t_1 increment. The NOE experiment was acquired using 24 (8) transients per t_1 increment. The initial t_1 sampling delay was adjusted for zero evolution or to half the dwell time in order to eliminate phase errors and baseline distortions (*30*).

A recycle delay of 2.6 s was used between t_1 increments for the R_1 and R_2 data sets for all complexes. A recycle delay of 4.6 s was used for all NOE measurements. Eleven time points were sampled for the T_2 relaxation decay at 6 (2×), 22, 42, 70 (2×), 122, 162, 202 (2×), and 333 ms (where 2× represents a duplicate measurement; 6 (2×), 10, 22 (2×), 42, 58, 90 (2×), 122, 162, 202, 298 (2×) ms for the binary data set). The same T_1 relaxation delay time points were applied as described for the ternary folate−DHNADPH complex (*23*), i.e., 10, 50, 100, 200, 400, 700, 1000, 1500, 2000, and 3000 ms. Duplicate data sets were acquired for T_1 delays of 10, 400, and 1500 ms (binary data set T_1 delays: 10 (2×), 60 (2×), 120, 200, 300, 480 (2×), 720, 1200, 1800, 2400 (2×) ms).

For the $^1H-^{15}N$ steady-state heteronuclear NOE measurements, two spectra, acquired with or without proton presaturation (corresponding to the presence and absence of the $^1H-^{15}N$ NOE, respectively) were recorded in an interleaved manner in order to minimize systematic differences between the two. A total of four pairs of spectra was acquired for the E:folate:$NADP^+$ and E:folate:DHNADPH complexes, and five pairs were acquired for the E:folate complex.

Spectral Processing. Spectra were processed with Felix95 (Molecular Simulations, Inc.) or NMRPipe (*31*) and visualized with Felix95 or NMRView (*32*) on a Silicon Graphics O2 workstation. All spectra within a relaxation time series were processed with identical parameters. Time−domain data were zero-filled once and apodized with an exponential window function or a shifted cosine-squared window function, depending on the extent of overlap. For the steady-state NOE spectra, solvent suppression was achieved via postacquisition convolution of the time−domain data (*33*).

Peak heights were measured using in-house macros. Uncertainties in the measured peak heights for the R_1 and R_2 measurements were estimated from the duplicate data sets as described previously (*23*). Uncertainties for the steady-state NOE were estimated from uncertainties in the peak intensities. Values for R_1 and R_2 and their uncertainties were determined by nonlinear least-squares fitting of the experimental data to monoexponential functions as described previously (*23*, *34*, *35*).

NMR Relaxation Data Analysis. The relaxation of the ^{15}N spin is dominated by dipolar and chemical shift anisotropy (CSA) interactions when the effects of cross-correlation are suppressed. Their relations to the spectral density, $J(\omega)$, are given by (*36*)

$$1/T_1 = (d^2/4)[J(\omega_H - \omega_N) + 3J(\omega_N) + 6J(\omega_H + \omega_N)] + c^2J(\omega_N) \quad (1)$$

$$1/T_2 = (d^2/8)[4J(0) + J(\omega_H - \omega_N) + 3J(\omega_N) + 6J(\omega_H + \omega_N) + 6J(\omega_H)] + (c^2/6)[4J(0) + 3J(\omega_N)] + R_{ex} \quad (2)$$

$$\mathrm{NOE} = 1 + ((d^2T_1)/4)(\gamma_H/\gamma_N)[6J(\omega_H + \omega_N) - J(\omega_H - \omega_N)] \quad (3)$$

in which $d = (\mu_0\hbar\gamma_H\gamma_N/8\pi^2)\langle r_{NH}^{-3}\rangle$; $c = \omega_N\Delta\sigma/(3)^{1/2}$; μ_0 is the permeability of free space; $\hbar$ is Planck's constant; γ_H and γ_N are the gyromagnetic ratios of ^{1}H and ^{15}N; r_{NH} is the N−H bond length (set to 1.02 Å); $\Delta\sigma$ is the CSA, which was set to −170 ppm (*37*); and ω_H and ω_N are the Larmor frequencies of ^{1}H and ^{15}N, respectively. R_{ex} is a parameter introduced to account for processes that contribute to T_2. R_{ex} is often interpreted as originating from motions on the millisecond/microsecond time scales. Unfortunately, if the rotational diffusion of the molecule is not isotropic, then changes in R_2 (and R_1) can occur, depending on the orientation of the N−H bond vector with respect to the principal axis frame of the diffusion tensor. These effects can lead to artifactual R_{ex} terms in model-free analysis when isotropic overall tumbling is assumed (*23*). In fact, detailed analyses of relaxation data from complexes involving DHFR have shown that anisotropic rotational diffusion introduces erroneous R_{ex} terms for ~50% of the analyzed spins (*23*).

If the degree of axial asymmetry is known, the amplitudes and time scales of the intramolecular motions of the N−H bond vectors can be extracted from the relaxation data using a modified model-free spectral density function:

$$J(\omega) = \frac{2}{5}\left\{S^2\left[\sum_{k=1\ldots3}\frac{A_k\tau_k}{1+\omega^2{\tau_k}^2}\right] + (1-S^2)\left[\sum_{k=1\ldots3}\frac{A_k\tau_k'}{1+(\omega\tau_k')^2}\right]\right\} \quad (4)$$

in which $A_1 = (3/4)\sin^4\theta$, $A_2 = 3\sin^2\theta\cos^2\theta$, $A_3 = (3\cos^2\theta - 1)^2/4$, and the correlation times (τ_1, τ_2, and τ_3) depend on the rotational diffusion coefficients: $\tau_1 = (4D_{\|} + 2D_\perp)^{-1}$, $\tau_2 = (D_{\|} + 5D_\perp)^{-1}$, and $\tau_3 = (6D_\perp)^{-1}$. $D_\perp = D_{xx} = D_{yy}$ and $D_{\|} = D_{zz}$ are the unique diffusion coefficients for axial symmetry. The generalized order parameter (S^2) describes the amplitude of the internal motion and ranges from 0 for unrestricted motion to 1 for a fixed vector. τ_k' is the effective correlation time and is dependent on τ_e, the correlation time for internal motions ($\tau_e \ll \tau_k$): $\tau_k' = \tau_k\tau_e/(\tau_k + \tau_e)$.

Calculation of the Rotational Diffusion Tensor. An accurate description of rotational diffusion is necessary for extraction of reliable internal motional parameters from model-free analyses. For axially symmetric diffusion, the tensor can be determined from the relationship of the local diffusion coefficient ($D_i = \tau_{ci}^{-6}$) with the angles of the N−H bond vectors (θ) relative to the principal axes of the diffusion tensor ($D_{\|}$ and $D_\perp$) (*38*, *39*):

$$D_i = D_{iso} - (3\cos^2\theta - 1)(D_{\|} - D_\perp)/6 \quad (5)$$

where $D_{iso} = (2D_\perp + D_{\|})/2$, and D_i is the local diffusion coefficient. For these procedures to work, however, spins exhibiting slow motions must be excluded from the analysis, which is often difficult in the presence of anisotropy (*23*, *40*).

We applied the COPED (COmparison of Predicted and Experimental Diffusion tensors) procedure to identify genuine motions in the presence of tumbling anisotropy (*23*). Hydrodynamic calculations were performed using the in-house program MASH as described previously (*23*). The hydration shell was optimized by minimizing the error function Γ ($\Gamma = \Sigma\eta_i^2$), where η_i^2 is the χ^2 statistic used to estimate the goodness of fit between the experimental local diffusion coefficient ($D_{i(expt)}$) and the predicted local diffusion coefficient ($D_{i(pred)}$): $\eta_i^2 = (D_{i(expt)} - D_{i(pred)}/\sigma_i)$. $D_{i(pred)}$, where σ_i is the uncertainty in $D_{i(expt)}$, was obtained from solution of the linear relation (eq 5) for values of D_{iso} and θ obtained from the hydrodynamics calculations. Values of $D_{i(expt)}$ and σ_i were determined from T_1/T_2 ratios as described by Lee et al. (*38*). The COPED analysis was applied to all three DHFR complexes. The structural coordinates represented by Protein Data Bank entry 1rx7 (*10*) were used for E:folate and E:folate:DHNADPH, and 1rx2 was used for E:folate:NADP$^+$ for the hydrodynamic calculations. A detailed description of the COPED analysis of the relaxation data for E:folate:DHNADPH has been reported elsewhere (*23*).

For all three complexes, spins exhibiting $\eta_i^2 > 15$ were identified as having slow motions. The principal components of the diffusion tensor that were used as input for the axially symmetric model-free analysis were calculated using the local diffusion approach (*38*). Residues exhibiting significant internal motions identified from the COPED analysis were excluded from these calculations. *F*-statistical testing was used to evaluate the significance of the isotropic, axially symmetric, and anisotropic tensor models in the analysis.

Axially Symmetric Model-Free Analysis. The relaxation data sets for the three complexes were fit to the axially symmetric model-free spectral density function (eq 4) using the program Modelfree (version 4.01; http://cpmcnet.columbia.edu/dept/gsas/biochem/labs/palmer/software.html) as described previously. Briefly, the relaxation data were fit to five extended Lipari−Szabo dynamic models for initial values of $D_\perp$, $D_{\|}$, and θ, determined from the local diffusion approach. The models considered were (1) S^2 only, (2) S^2 and τ_e, (3) S^2 and R_{ex} (a term used to describe the contributions of microsecond/millisecond time scale motions to T_2), (4) model 2 plus R_{ex}, and (5) the extended two-time scale model (*41*).

The best model for each spin was determined from *F*-statistical testing as described by Mandel et al. (*42*). After model selection, a final optimization was performed in which parameters describing the axially symmetric diffusion tensor were optimized for the appropriate model for each spin.

Back-Calculated NOESY Spectra. 3D ^{15}N-edited NOESY spectra were simulated using the program SPIRIT (*43*) for structural coordinates representative of the occluded, closed, and open conformations of the DHFR complexes represented by PDB accession codes 1rx7, 1rx2, and 1ra2, respectively (*10*). This analysis was performed as a method to quickly identify the conformation of the Met20 loop in the E:folate:DHNADPH complex. Accordingly, only residues expected to exhibit NOEs to residues in the Met20 loop were included.

RESULTS

NMR Relaxation Data and COPED Analysis. Representative ^{1}H−^{15}N HSQC spectra of the three DHFR complexes are shown in Figure 2. Because of spectral overlap or broadening, some resonances were not sufficiently resolved for accurate measurement of peak intensity. Relaxation data could be obtained for 138, 115, and 112 of the non-proline residues in the E:folate, E:folate:DHNADPH, and E:folate:NADP$^+$ complexes, respectively (Figure 3).

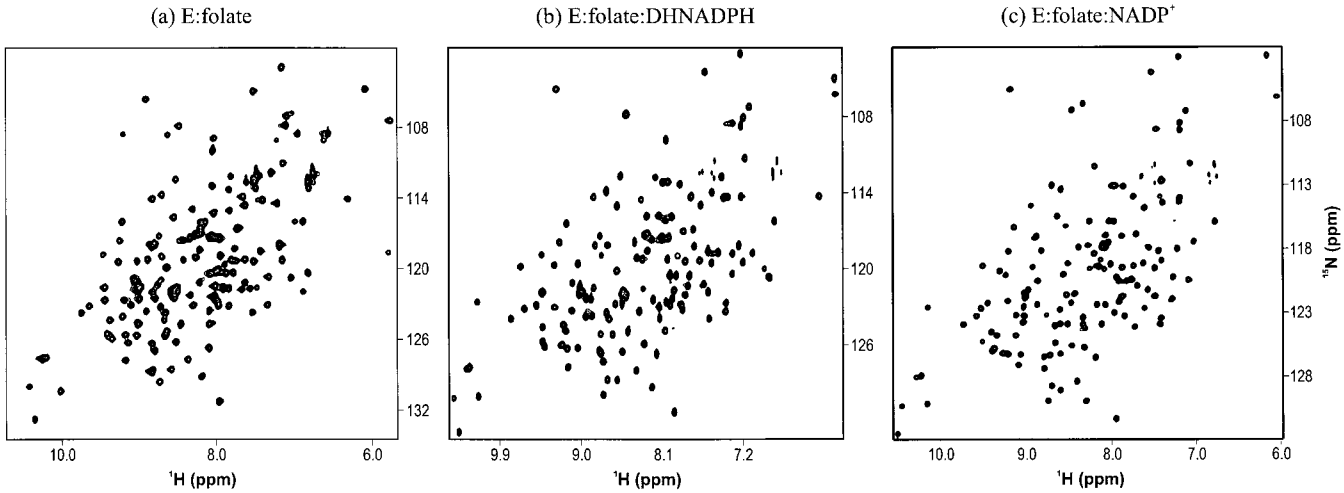

FIGURE 2: Representative $^{1}H-^{15}N$ HSQC spectra of the three DHFR complexes: (a) E:folate, (b) E:folate:DHNADPH, and (c) E:folate:NADP^{+}.

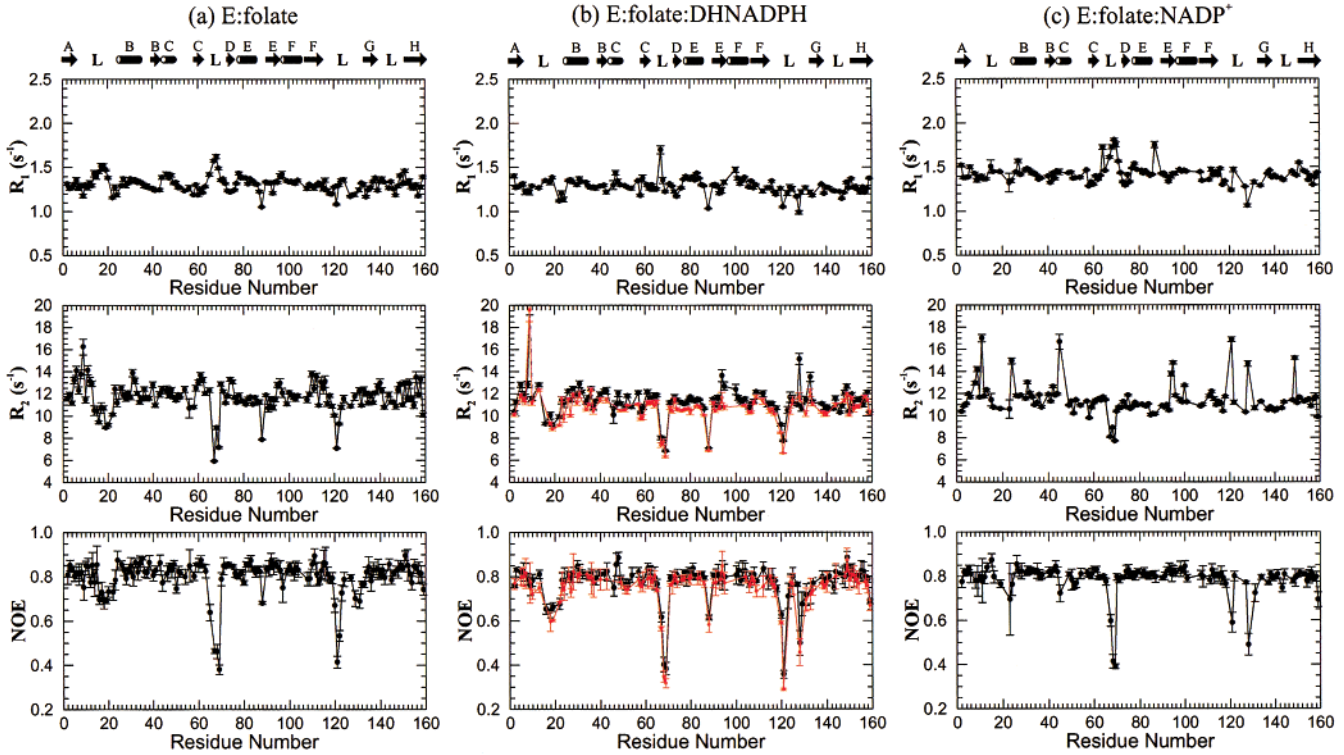

FIGURE 3: ^{15}N Relaxation data for the three DHFR complexes: (a) E:folate, (b) E:folate:DHNADPH, and (c) E:folate:NADP^{+}. R_1, R_2, and $^{1}H-^{15}N$ NOE data sets were collected at 600 MHz for all complexes. R_2 and NOE data sets were additionally acquired for the E:folate:DHNADPH complex at 500 MHz (red data points).

We have shown previously that failure to account for anisotropic tumbling results in erroneous model selection in model-free analysis of relaxation data for complexes of DHFR (*23*). The experimental relaxation data for the DHFR complexes studied in the present work were therefore analyzed using the COPED procedure to identify a subset of residues that can be used to accurately define the diffusion tensor (*23*). The results of the COPED analyses for the three DHFR complexes are shown in Figure 4. To minimize the function, Γ, the C^{α} atom bead radii were set to 3.16, 3.19, and 3.05 Å for the E:folate, E:folate:DHNADPH, and E:folate:NADP^{+} complexes, respectively. The smaller radius for E:folate:NADP^{+} reflects its shorter rotational correlation time, which is most likely a consequence of decreased viscosity due to the lower concentration of this sample (ca. 1.2 mM as compared to ca. 1.7 mM for the other complexes). However, the magnitude of the anisotropy predicted from the hydrodynamics analysis is similar for the three complexes (Table 1).

In general, there is excellent agreement between the predicted and the experimental local diffusion coefficients for all three complexes (Figure 4), i.e., most of the experimental D_i values lie close to the values predicted from hydrodynamic modeling (represented by the straight lines). This suggests that the X-ray structures used for the diffusion analyses accurately represent the solution structures and also indicates that fast motions dominate. Experimental diffusion coefficients that lie significantly below the expected theoreti-

Table 1: Summary of Diffusion Parameters for DHFR Complexes

	COPED			quadric diffusion[a,b]			model-free			
complex	bead radius (Å)	$\tau_{m\,iso}$[c] (ns)	$D_{\|/\perp}$	$\tau_{m\,iso}$[c] (ns)	$D_{\|/\perp}$	F[d]	$\tau_{m\,iso}$[c] (ns)	$D_{\|/\perp}$	θ[e]	ϕ[e]
E:folate[f,g]	3.16	8.98	1.15	9.03	1.15	32	9.03	1.15	0.50	0.12
E:folate:DHNADPH[f,h]	3.19	9.05	1.15	9.01	1.18	70	9.05	1.18	1.56	4.80
E:folate:NADP$^+$[i,j]	3.05	8.42	1.16	8.43	1.18	70	8.44	1.17	2.10	1.82

[a] Determined using the quadric diffusion program of Lee et al. (*37*). [b] Residues undergoing motions were excluded from these analyses if they exhibited $\eta_i^2 > 15$ in the COPED analyses. [c] Effective isotropic correlation time. [d] Values given with respect to the isotropic and axially symmetric diffusion tensor models. [e] Values given with respect to the inertial tensor frame. [f] PDB coordinates 1rx7 (occluded) were used in these analyses. [g] Values of $D_{i(expt)}$ for 109 residues identified from COPED were fit using quadric diffusion. [h] Values of $D_{i(expt)}$ for 96 residues identified from COPED were fit using quadric diffusion. [i] PDB coordinates 1rx2 (closed) were used in these analyses. [j] Values of $D_{i(expt)}$ for 74 residues identified from COPED were fit using quadric diffusion.

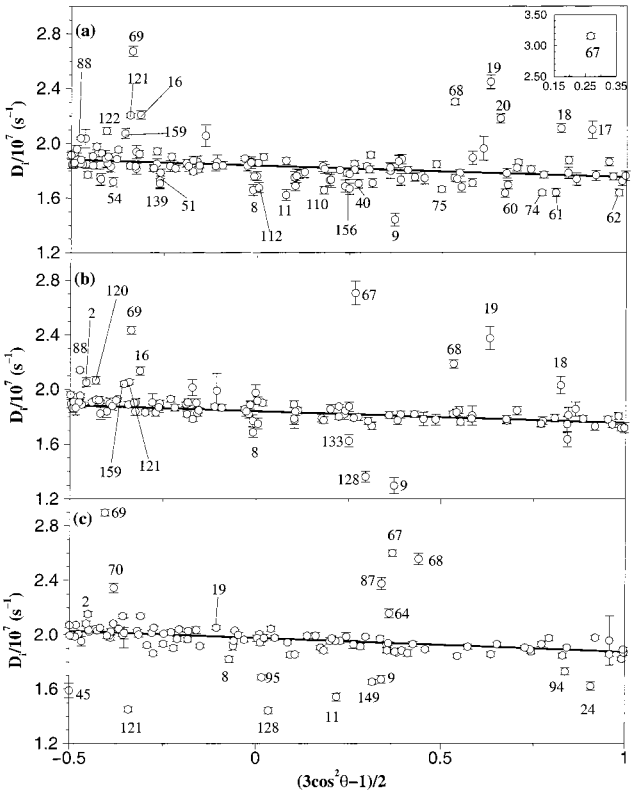

FIGURE 4: Graphical representation of the COPED analyses for the DHFR complexes: (a) E:folate, (b) E:folate:DHNADPH, and (c) E:folate:NADP$^+$. Residues most likely to exhibit slow motions on the nanosecond (above the solid line) and millisecond/microsecond time scales (below the solid line) are indicated.

cal values represent residues that are subject to slow millisecond/microsecond time scale motions; these residues were excluded from the diffusion tensor calculations. Residues that exhibit local D_i values much greater than predicted from the hydrodynamics analysis are those for which nanosecond time scale motions contribute to the ^{15}N relaxation. Many of these residues have been identified in Figure 4 by their position in the amino acid sequence.

Calculation of Diffusion Tensors. The degree of rotational diffusion anisotropy for the three complexes was determined using the local diffusion approach of Lee et al. (*38*). Residues identified as undergoing slow time scale motions from COPED were excluded from these calculations. The refined diffusion parameters for the three DHFR complexes are summarized in Table 1. *F*-statistical testing (Table 1) indicates that an axially symmetric diffusion tensor, rather than an isotropic tumbling model, better describes the relaxation data for all three complexes. The degree of anisotropy is very similar for each of the three complexes ($D_{\|/\perp} = 1.15-1.18$). The small differences observed in the effective isotropic correlation times (Table 1) are likely due to differences in protein concentration, which can affect the viscosity (*23*, *44*).

Backbone Dynamics. The dynamics parameters extracted using the axially symmetric model-free spectral density function of Lipari and Szabo (*45*, *46*) for the three complexes of DHFR are plotted as a function of residue number in Figure 5. The final, optimized diffusion tensors are given in Table 1 and show little difference between the three complexes. The relaxation data could be adequately described by one of the five dynamical models for the majority of residues.

Simulation of E:Folate:DHNADPH NOESY Spectrum. Strips taken from the experimental ^{15}N-edited NOESY spectrum of E:folate:DHNADPH were compared with spectra simulated using the program SPIRIT (Figure 6). Simulated spectra for the open Met20 loop conformation are in poor agreement with experiment and are not shown. There are 19 NOE cross-peaks that differentiate the occluded conformation (shown in red in Figure 6) from the closed X-ray conformation (colored green; see figure legend for further details). All but one of the NOE cross-peaks characteristic of the occluded conformation are observed in the experimental spectrum of the E:folate:DHNADPH complex, while no experimental NOE cross-peaks are observed that are diagnostic of the closed conformation. Thus, the pattern of NOEs observed in the experimental NOESY spectrum for the E:folate:DHNADPH complex strongly suggest that the Met20 loop is predominantly in the occluded conformation.

DISCUSSION

Protein Conformation. Detailed interpretation of the dynamic data reported here requires knowledge of the conformational differences between the E:folate, E:folate:DHNADPH, and E:folate:NADP$^+$ complexes. From their analyses of the X-ray structures of numerous complexes of *E. coli* DHFR, Sawaya and Kraut (*10*) have identified three conformations of the Met20 loop, termed open, closed, and occluded (Figure 7). In space groups where lattice contacts involving the Met20 loop are weak, ligand-dependent conformational changes between the closed and the occluded structures are observed that reflect the intrinsic structural preferences of the protein. The occluded conformation is observed only when the binding pocket for the nicotinamide ring of the cofactor is empty. In this conformation, residues

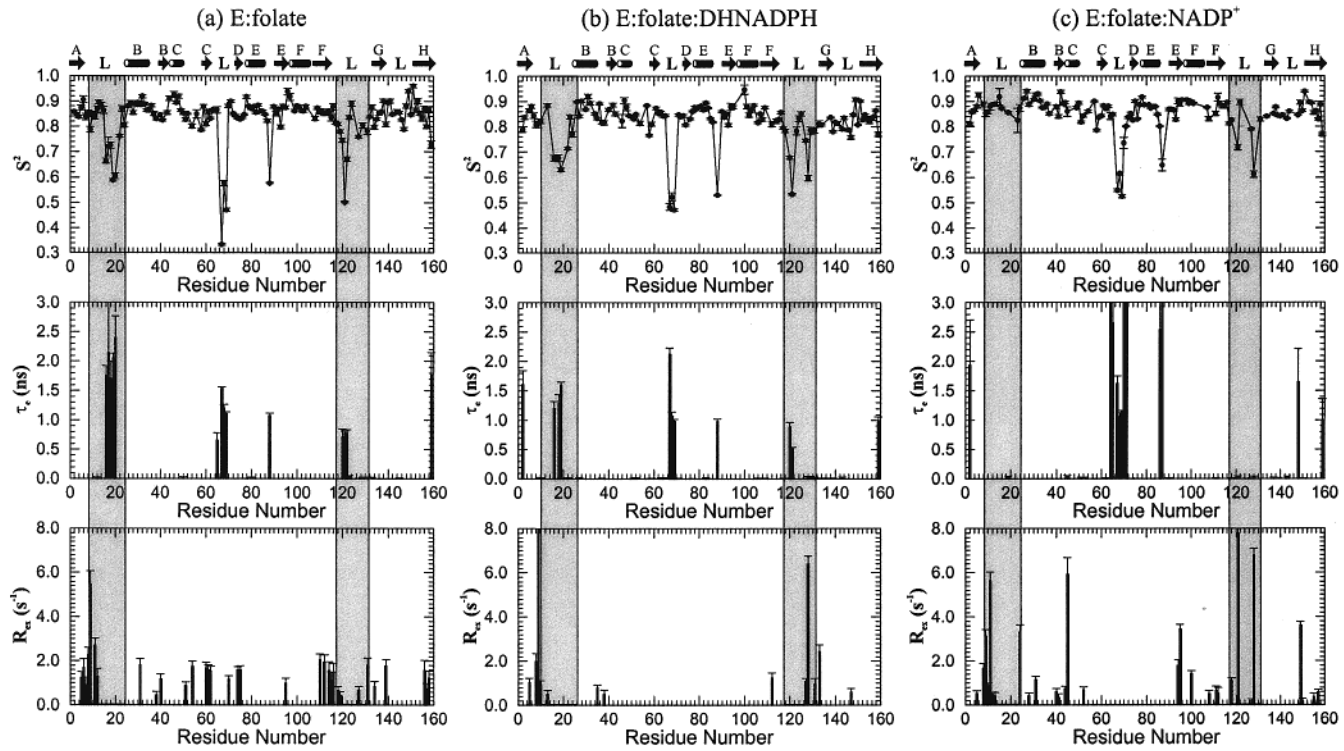

FIGURE 5: Dynamics parameters for the three DHFR complexes extracted using the axially symmetric model-free analysis. Values for R_{ex} are reported at 600 MHz. Residues comprising the Met20 loop and the F−G loop are highlighted.

14−16 in the Met20 loop protrude into the nicotinamide binding pocket (*10*). In the closed conformation, the Met20 loop packs tightly against the nicotinamide−ribose moiety of the cofactor and seals the active site. These loop transitions are accompanied by changes in hydrogen bonding (Figure 7b). The closed conformation of the loop is stabilized by hydrogen bonds from Gly15 and Glu17 in the Met20 loop to Asp122 in the F−G loop. These hydrogen bonds are broken in the occluded conformation, and new hydrogen bonds are formed between Asn23 at the end of the Met20 loop and Ser148 in the G−H loop (*10*).

The E:folate complex adopts the occluded conformation in all space groups in which the Met20 loop conformation is not influenced by strong crystal packing interactions. In the crystal structure of the E:folate:$NADP^+$ complex, the Met20 loop is closed with the nicotinamide ring located in the binding pocket in close proximity to the pterin ring of the folate substrate analogue. Detailed analyses of the NMR chemical shifts for several complexes of DHFR have led to the identification of a set of marker resonances that are diagnostic of the conformation of the Met20 loop and of the presence of the nicotinamide ring in the binding pocket.[2] In the particular case of the E:folate and E:folate:$NADP^+$ complexes, the chemical shifts confirm that the Met20 loop is occluded and closed, respectively, in solution and show that conformational differences are localized to the Met20, F−G, and G−H loop regions. No X-ray structure has been reported for the E:folate:DHNADPH complex; however, in the structure of the closely related NADPH:dideazatetrahydrofolate complex, the Met20 loop is occluded, and the nicotinamide ring projects out of the pocket toward the solvent and is disordered (*10*). The NMR marker resonances indicate that the Met20 loop adopts the occluded conformation in E:folate:DHNADPH in solution, which on the basis of the X-ray structures (*10*) would exclude the nicotinamide ring from the binding pocket. The chemical shift of the NH resonance of Ala7, which hydrogen bonds to the carboxamide group of the cofactor in the closed E:NADPH and E:folate:$NADP^+$ complexes (*10*), confirms exclusion of the nicotinamide ring from the binding pocket in E:folate:DHNADPH in solution.[2] In addition, a ^{13}C-edited, ^{13}C-filtered NOESY spectrum (*25*) of the complex formed between $^{15}N/^{13}C$-labeled DHFR and unlabeled folate and DHNADPH shows none of the intermolecular NOEs that would be expected if the nicotinamide ring was in the active site (data not shown). Finally, simulations of the NOESY spectrum of E:folate:DHNADPH performed using the program SPIRIT show excellent agreement between the experimental spectrum and that calculated from the occluded X-ray structure but poor agreement with those calculated from either the open or the closed conformations (Figure 6).

Dynamics of the Occluded Complexes (E:Folate and E:Folate:DHNADPH). Inspection of Figure 5 shows that the dynamic features of the E:folate and E:folate:DHNADPH complexes, both of which adopt the occluded Met20 loop conformation, are very similar. The average S^2 values in elements of regular secondary structure are very similar for both complexes, with an average over all secondary structural elements of 0.85. Compared to this average value, significantly decreased values of S^2, together with large values for the internal correlation time τ_e, are observed in many of the loops, indicating increased motions on the picosecond/nanosecond time scale in these regions. The location of these flexible loops on the structure is shown in Figure 8. Most notable is the enhanced flexibility in the Met20 loop (residues 16−22), in the adenosine binding loop (residues 67−69), and in the F−G loop (residues 119−123). Motions are also evident for residues 127−133, as indicated by slightly

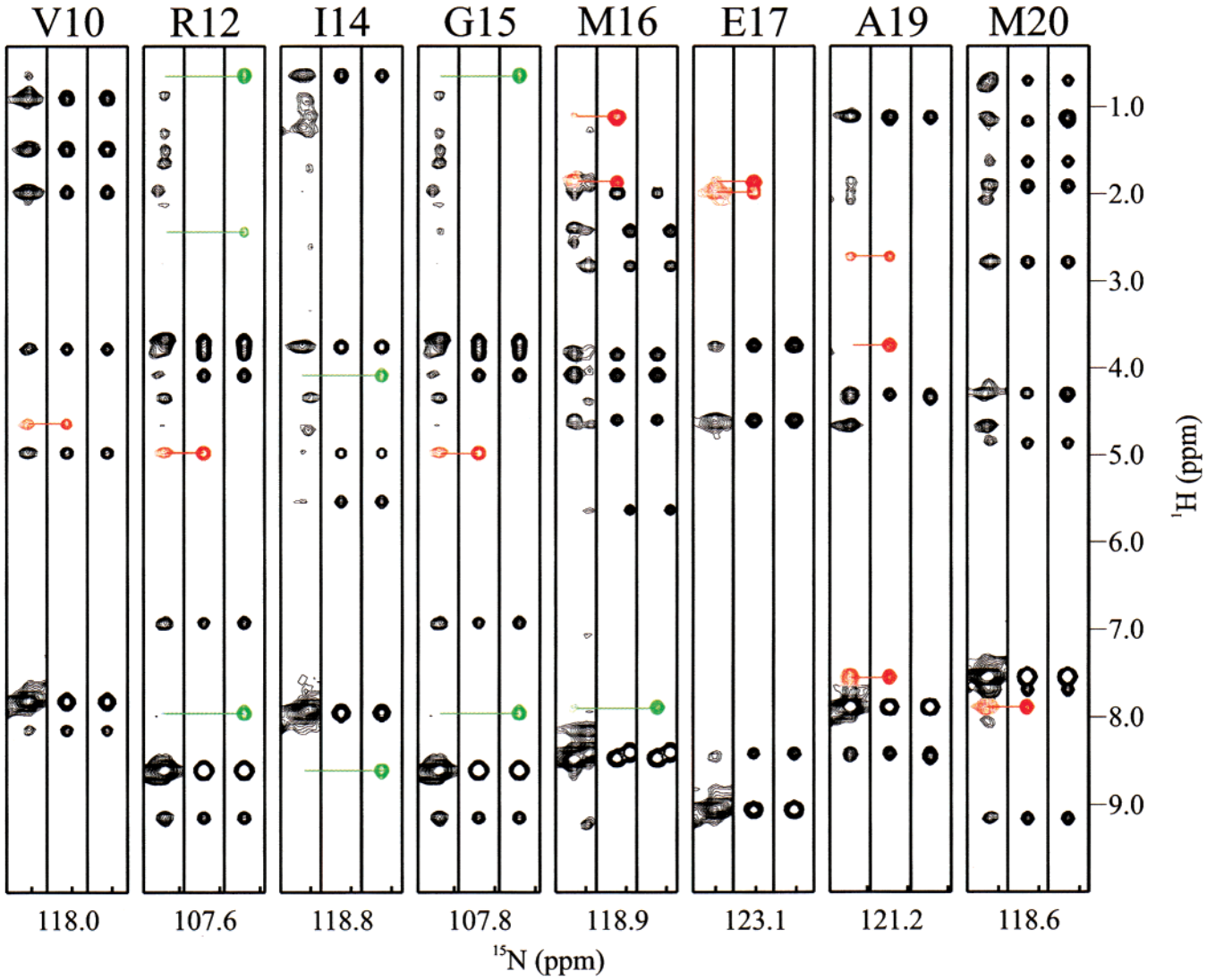

FIGURE 6: Comparisons of the back-calculated 3D ^{15}N-edited NOESY spectra from the occluded and closed conformations of DHFR and the experimental spectrum of the E:folate:DHNADPH complex. ^{1}H−^{1}H strips taken at ^{15}N frequencies of selected residues in the Met20 loop are shown for the experimental NOESY spectrum (left column), the occluded conformation (middle column), and the closed conformation (right column) for each residue. The simulated spectra were calculated using the program SPIRIT (*43*) from the coordinate files 1rx7 (occluded) and 1rx2 (closed). Cross-peaks that are characteristic of the occluded conformation are shown in red, while those that are diagnostic of the closed conformation of the Met20 loop are indicated in green.

decreased S^2 and small τ_e values. A significantly decreased S^2 is observed for Tyr128 in E:folate:DHNADPH; however, no data are available for this residue in the E:folate complex because of overlap with Arg57. Finally, Val88 displays a small S^2 and large τ_e for both of the complexes: this residue functions as a hinge between the adenosine binding domain and the major domain (*47*). Thus, several of the critical loops implicated in the catalytic function of DHFR display large amplitude motions on the picosecond/nanosecond time scale.

Evidence for microsecond/millisecond time scale motions in the F−G loop and at the beginning of the Met20 loop comes from the R_{ex} terms (Figure 5). Large values for R_{ex} (>5.5 s^{-1}) are observed for Ala9 in both occluded complexes and for Tyr128 in the E:folate:DHNADPH complex (Tyr128 is overlapped in the E:folate complex so no comparative data could be obtained). Given their magnitude, that they are conserved in all three complexes, and that anisotropic diffusion tensors were used for the model-free analysis, we can be confident that these exchange terms arise from slow conformational fluctuations rather than inappropriate choice of isotropic tumbling models. (The significance of the many small R_{ex} terms observed in the E:folate complex is being examined by detailed $T_{1\rho}$ measurements that will be reported elsewhere.)

In general, the trends in the S^2 parameters and internal correlation times for E:folate derived from the new relaxation data reported here are very similar to those obtained earlier (*5*). However, the new data are more precise, and the use of gradient flip-back methods eliminates potential artifacts arising from the use of spin-lock purge pulses for solvent suppression in the earlier work. The trends in S^2 values are similar in the two analyses; however, in the particular case of the hinge residue K38, the diminished S^2 value found in the earlier study could not be reproduced. Finally, many of the R_{ex} terms in the original analysis are now known to be artifacts due to assumption of an isotropic tumbling model.

It is of interest that the E:folate and E:folate:DHNADPH complexes have very similar backbone dynamics. In particular, the picosecond/nanosecond time scale backbone dynamics of both the cofactor binding site and the substrate

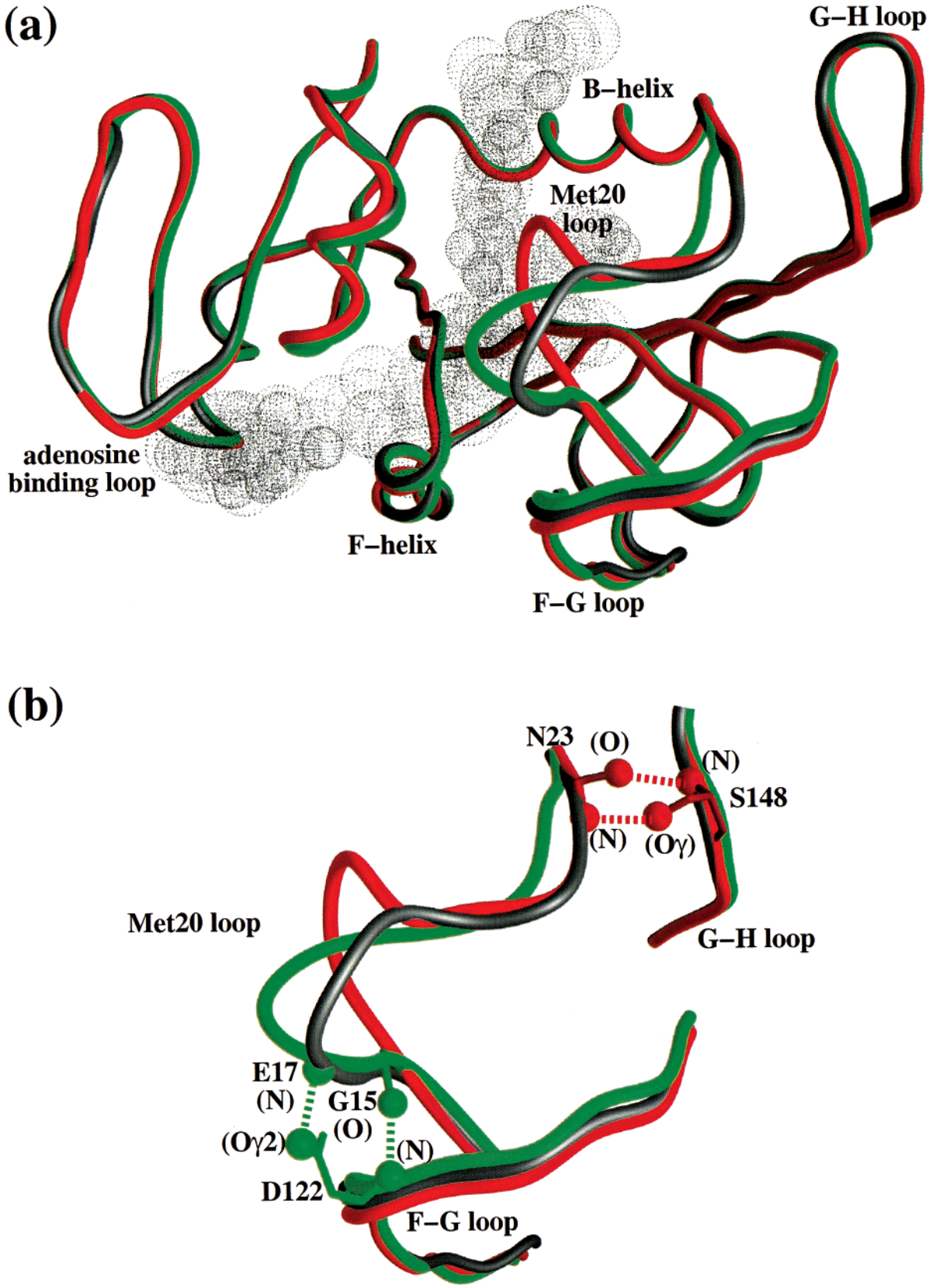

FIGURE 7: (a) Overlay of the α-carbon traces for the three crystallographically observable conformations of *E. coli* DHFR (*10*). The conformations are distinguished according to the orientations of the Met20 loop as: closed (green), open (gray), and occluded (red). The bound folate and cofactor are represented as dot surfaces. (b) Close-up view of the Met20 loop and its interactions with the F−G and G−H loops. Coordinates representing the three conformations were taken from the Brookhaven database and are 1rx2 (closed), 1rx7 (occluded), and 1ra2 (open). The structures were generated using the program GRASP (*58*).

binding site are insensitive to the presence or absence of bound NADPH. Thus, the principal determinant of backbone dynamics in these complexes is the occluded conformation of the Met20 loop rather than the nature of the bound ligands.

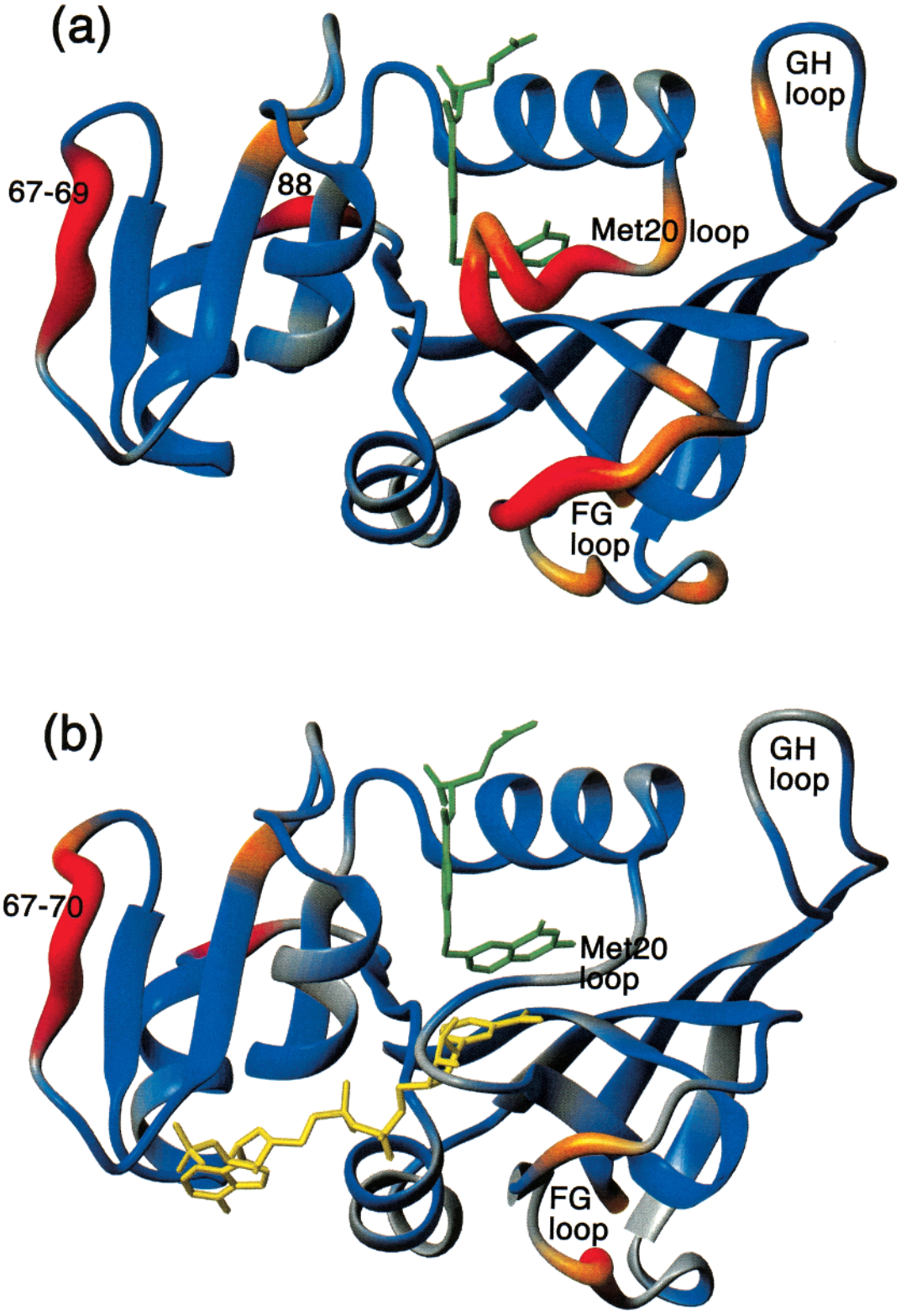

FIGURE 8: Ribbon diagram of DHFR showing the location of regions in which there are enhanced motions on the picosecond/nanosecond time scale in (a) the occluded E:folate binary complex and (b) the closed E:folate:NADP$^+$ complex. The ribbon is color coded to indicate S^2 values: $S^2 > 0.8$, blue; $0.71 < S^2 < 0.8$, orange; $S^2 < 0.70$, red. The radius of the ribbon is also increased to reflect the decrease in S^2 values. The figures were generated using the program MOLMOL (*59*) from the X-ray coordinate sets 1rx7 and 1rx2 (*10*).

That is not to say that binding of substrate or cofactor is completely without influence on backbone dynamics: exchange between two distinct conformations of the Met20 loop (at a rate of ca. 35 s^{-1}) has been observed for the apo enzyme (*6*), and this process is clearly abrogated or moved to a faster time scale by binding of cofactor and/or substrate.

Dynamics of the Closed Complex (*E:Folate:NADP*$^+$). The picosecond/nanosecond time scale backbone dynamics of the closed E:folate:NADP$^+$ complex differ strikingly from that of the two occluded complexes in several regions (Figures 5 and 8). The S^2 values in elements of regular secondary structure (0.87 average) are similar to those of the other two

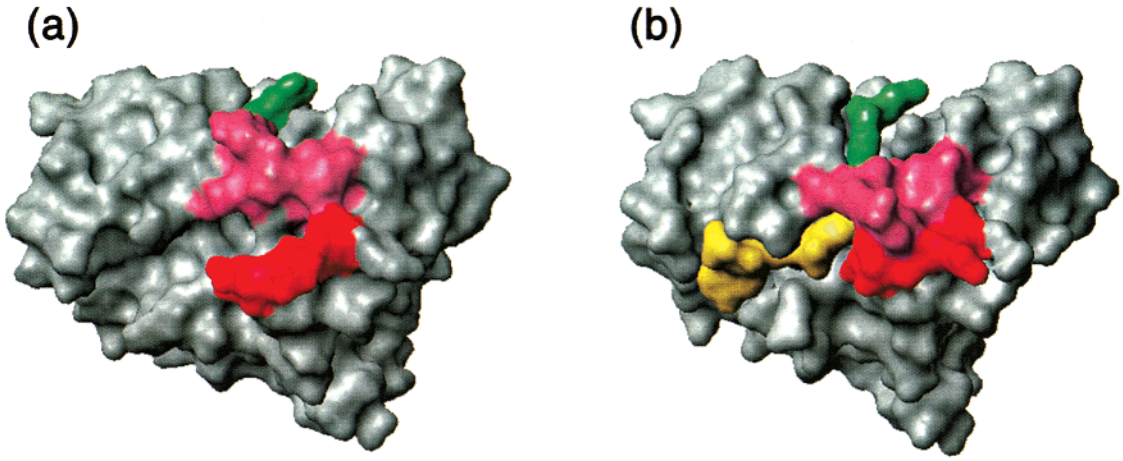

FIGURE 9: Surface representations of DHFR, indicating the differences in packing between the Met20 and the F−G loops in the occluded (a) and closed (b) structures. The surface formed by residues 16−22 in the Met20 loop is shown in pink, and that formed by residues 119−123 in the F−G loop is colored red. These residues undergo large amplitude fluctuations on the picosecond/nanosecond time scale in the occluded E:folate and E:folate:DHNADPH complexes, which are damped in the closed E:folate:$NADP^+$ complex. The surface of the bound folate is colored green, and that of the $NADP^+$ in the E:folate:$NADP^+$ complex is yellow.

complexes, showing that the backbone motions of the central framework are unchanged. However, the large amplitude motions observed in the occluded complexes in the Met20 loop and for residues 119−123 in the F−G loop are largely attenuated in the E:folate:$NADP^+$ complex, as indicated by the increased S^2 and decreased τ_e values in these regions. Indeed, the average S^2 for the entire Met20 loop (residues 9−24) increases from 0.75 to 0.87 between the E:folate:DHNADPH and the E:folate:$NADP^+$ complexes. Similarly, the average S^2 for the F−G loop (residues 117−131) increases from 0.70 to 0.80 in the same two complexes. These striking differences in flexibility for residues in the Met20 and F−G loops can be readily understood on the basis of the X-ray structures (*10*). In the occluded complexes, the conformation of the Met20 loop is such that residues 14−16 penetrate the unoccupied nicotinamide binding pocket. The entire loop from Met16−Trp22 is solvent exposed with few contacts with other regions of the protein (Figure 9). Similarly, residues 119−123 in the F−G loop project from the protein into the solvent and make no contacts with neighboring regions. Thus, the high flexibility observed for these loops in the occluded configuration is not surprising. The transition to the closed conformation, however, results in close packing interactions between the Met20 loop and the F−G loop (Figure 9). In addition, residues 18−20 pack tightly against the cofactor (*10*). The close packing plus the hydrogen bonds formed between the Met20 and the F−G loops, shown in Figure 7b, are the most probable origins of the greatly reduced flexibility observed in the closed E:folate:$NADP^+$ complex.

The adenosine binding loop remains highly mobile in the E:folate:$NADP^+$ complex. S^2 values are very similar to those in E:folate:DHNADPH, but the backbone motions are more complex, and the two-time scale model (model 5) is required to fit the relaxation data for many more residues. Thus, significant τ_e terms are observed only for residues 67−69 in the occluded complexes, whereas large τ_e values are found for residues 64−72 in E:folate:$NADP^+$ (Figure 5), indicating the presence of more extensive nanosecond time scale backbone motions that encompass the entire loop. It is of great interest that a conformational change that affects only the Met20, F−G, and G−H loops is transmitted to a distant site (the adenosine binding loop, more than 18 Å away) in the form of altered backbone dynamics. We note that motional coupling between the adenosine binding loop and the Met20 loop has been observed in molecular dynamics simulations of DHFR (*22*). Furthermore, coupling of residues 63−68 to distant regions of the protein, including the substrate binding site, has been predicted from ensemble-based computer modeling (*48*). Enhanced flexibility is also evident in the hinge, near Val88. Although data cannot be obtained for residue 88 itself, due to overlap, the small S^2 for Asp87 and large τ_e values for both Gly86 and Asp87 reveal the presence of picosecond/nanosecond time scale motions in the hinge region of E:folate:$NADP^+$. Finally, the order parameters reveal the retention of flexibility for Asp127 and Tyr128 in the F−G loop.

While residues 67−69 and 88 display unusual dynamic parameters relative to the rest of the protein, these parameters do not vary significantly among the three complexes studied. This suggests that the motions of these residues change little in the different conformational states and complexes of the enzyme and may consequently have little bearing on catalysis. This is supported by the fact that the Gly67Val DHFR mutant and deletion mutants of Gly67 and Val88 exhibit unperturbed binding of both substrates and have rate constants for hydride transfer that are similar to wild-type DHFR (*49*, *50*). Consequently, a number of residues within the protein that are key for catalysis, but may not otherwise be identified as such, may be recognized as those whose dynamics change from complex to complex within the reaction cycle.

Differences in microsecond/millisecond time scale motions are also evident from significant changes in the R_{ex} terms between the E:folate:$NADP^+$ and E:folate or the E:folate:DHNADPH complexes. In the E:folate:$NADP^+$ complex, Leu24 has an exchange term of 3.3 s^{-1}, whereas its relaxation data can be fit by fast motional models (model 1), without the need for exchange terms, in the two occluded complexes. Similarly, exchange contributions are required for His149 in E:folate:$NADP^+$ but are not required for the occluded complex. We also note a large τ_e for Ser148 in the E:folate:

$NADP^+$ complex, indicating new motions on the nanosecond time scale that are absent from the other species. These differences in dynamics appear to be related to the structural changes that are known to accompany the occluded to closed transition. With the Met20 loop in the occluded conformation, a pair of hydrogen bonds is formed between the backbone NH and CO of Asn23 and the O^γ and backbone NH of Ser148 (Figure 7b); these hydrogen bonds are broken in the closed configuration (*10*). Thus, although the present data provide no insights into the detailed mechanism, it seems that breaking of these hydrogen bonds between the Met20 and the G−H loop permits slow time scale conformational fluctuations that influence the ^{15}N T_2 relaxation of Leu24 and His149 and allows new nanosecond time scale motions for Ser148.

A large R_{ex} term (7.8 s^{-1}) is required for G121 in the E:folate:$NADP^+$ complex and is also associated with hydrogen bonding changes that accompany the occluded to closed transition. In the closed conformation, a pair of hydrogen bonds is formed from the Gly15 CO and Glu17 NH in the Met20 loop to the backbone NH and side chain carboxyl of Asp122 in the F−G loop (*10*). These hydrogen bonds are broken in the occluded conformation (Figure 7b). The NMR data suggest the presence of slow conformational fluctuations in the closed form that affect the ^{15}N T_2 relaxation of Gly121.

It is notable that the ^{15}N resonances of residues Leu24, Gly121, and His149, which display substantial R_{ex} terms in E:folate:$NADP^+$, undergo substantial chemical shift changes (>2 ppm) between the closed and occluded conformations.[2] Thus, it is possible that the exchange contributions to the T_2 relaxation of these nuclei arise from transient fluctuations from the closed to the occluded conformation, at least insofar as it affects the hydrogen bonding interactions between the Met20 and the F−G and the G−H loops.

Substantial R_{ex} terms are observed for Ile94, Gly95, and Tyr100 in the E:folate:$NADP^+$ complex. These residues are in contact with the pterin ring (Ile94) and nicotinamide ring (Gly95, Tyr100), and the exchange terms probably reflect slow time scale conformational fluctuations involving the substrate and nicotinamide ring of the bound $NADP^+$. Interestingly, these exchange terms are absent for the E:folate:DHNADPH complex, in which the Met20 loop is occluded and the nicotinamide ring is excluded from the binding pocket. Thus, the T_2 relaxation data point toward conformational fluctuations in the active site on a time scale comparable to that of hydride transfer (950 s^{-1}) (*17*).

Finally, a large R_{ex} term is observed for His45 in the E:folate:$NADP^+$ complex. The backbone amide and imidazole ring of His45 form hydrogen bonds to phosphate oxygen atoms of the bound cofactor (*10*). The large exchange terms probably reflect microsecond/millisecond time scale fluctuations within the adenosine binding pocket or even transient dissociation of the adenosine moiety itself, as would occur in the transition from the E:THF:$NADP^+$ ternary product complex to the E:THF species.

Modeling the Catalytic Cycle. On the basis of X-ray structures of numerous substrate/product analogue complexes and cofactor complexes, Sawaya and Kraut (*10*) have proposed that DHFR undergoes transitions between closed and occluded conformations during the reaction cycle. In the early stages of the reaction cycle (Figure 1), in the NADPH binary complex and the Michaelis complex, the Met20 loop is closed and the nicotinamide ring is bound within the active site pocket. The complexes formed in the latter part of the reaction cycle following hydride transfer—the E:THF:$NADP^+$ and E:THF product complexes and the E:THF:NADPH product release complex—are all proposed to be occluded.

Following the arguments of Sawaya and Kraut (*10*), we consider the three complexes studied in the present work to be representative of several of the species formed in the reaction cycle. The E:folate:$NADP^+$ ternary complex, which is in the closed conformation with the nicotinamide ring of the cofactor buried deeply in the active site, is considered to be a model of the Michaelis complex. The occluded E:folate complex is a good model for the binary E:THF product complex; direct NMR studies of the much less stable E:THF complex confirm that it is also in the occluded conformation.[2] The occluded E:folate:DHNADPH complex can be regarded as a model both for the product ternary complex (E:THF:$NADP^+$) and for the product release complex (E:THF:NADPH). The fact that the backbone dynamics are determined primarily by the nature of the Met20 loop conformation and are largely insensitive to the nature of the bound ligand gives us confidence in these assignments to particular species in the reaction pathway.

Finally, we consider that E:folate:DHNADPH is also a good model for a pre-Michaelis complex formed immediately after binding of the substrate dihydrofolate to the holoenzyme (E:NADPH). Such a species has been observed in the reaction pathway of DHFR mutants in which Gly121 has been substituted or deleted (*19*, *21*) and is associated with a conformational rearrangement involving the nicotinamide ring of NADPH. Although this conformational rearrangement can be resolved kinetically for the G121 mutants, it is not observed for the wild-type enzyme where it must occur rapidly. Recently, we have obtained direct NMR evidence that this rearrangement does occur in wild-type DHFR and involves insertion of the nicotinamide ring into the binding pocket.[2] The E:folate:DHNADPH complex is an excellent model for this pre-Michaelis complex, since the Met20 loop adopts the occluded conformation with the nicotinamide ring out of the binding pocket. Such a species would be catalytically inactive, implying that a conformational change, in which the nicotinamide ring is inserted into the binding pocket, must precede the chemical step of hydride transfer in the reaction cycle. Thus, the complexes studied in the present work model four species in the DHFR kinetic cycle (Figure 1), plus an inactive pre-Michaelis complex formed after the binding of substrate to the E:NADPH complex.

Role of Dynamics in the Catalytic Cycle. In the occluded complexes formed on the product side of the reaction cycle (Figure 1), large amplitude fluctuations are observed in regions of the Met20 loop and in the neighboring F−G loop in the immediate vicinity of Gly121 (Figures 5 and 8). The polypeptide backbone in these loops is thus extremely flexible on a picosecond/nanosecond time scale. Local high frequency fluctuations of the Met20 loop, with occasional large amplitude conformational fluctuations, probably play an important role in facilitating product release.

A plausible mechanism for NADPH-assisted product release, which is rate determining (*17*), involves transient

insertion of the nicotinamide ring of NADPH into its binding pocket within the occluded E:THF:NADPH product release complex (*10*). The X-ray structures show that there is overlap between the binding pockets for the nicotinamide and pterin rings and that the magnitude of the steric clash depends on the extent of ring pucker. The reduced nicotinamide ring has both an increased pucker and a greater tendency to occupy the binding pocket than the planar nicotinamide ring of $NADP^+$. Consequently, fluctuations of the Met20 loop that remove the occluding residues from the binding pocket would be expected to play a role in promoting NADPH-assisted THF release.

The high flexibility of the Met20 loop is likely to play an equally important role in the transition to catalytically competent species. In the occluded conformation adopted by the Met20 loop in the pre-Michaelis complex,[2] residues 14−16 occupy the nicotinamide binding pocket and prevent binding of the nicotinamide ring (*10*). Significant movements of the Met20 loop are essential if the nicotinamide ring of the cofactor is to access its binding pocket in the active site, an obvious prerequisite for hydride transfer. The observed flexibility of residues 16−22 in the occluded conformation is likely to play an important role in the gating action of the Met20 loop. Large amplitude backbone fluctuations on a nanosecond or faster time scale will facilitate slower backbone conformational transitions that result in open Met20 loop conformations that provide access to the active site. Thus, flexibility of the Met20 loop probably plays an essential role in promoting binding of the nicotinamide ring and formation of NACs in the Michaelis complex.

Movement of the nicotinamide ring into the active site in the Michaelis complex is expected to result in closure of the Met20 loop, as in the E:folate:$NADP^+$ complex (*10*). In the closed configuration, the Met20 loop is packed tightly against both the cofactor and the F−G loop, and its conformation is stabilized through formation of hydrogen bonds between the two loops (Figure 7b). The relaxation parameters for E:folate:$NADP^+$ show that the large amplitude picosecond/nanosecond time scale fluctuations of the Met20 loop and the neighboring F−G loop characteristic of the occluded conformation are now strongly attenuated, although R_{ex} terms suggest that there are still slow time scale fluctuations that affect these loops. Thus, in the Michaelis complex, the erstwhile flexible Met20 loop closes over the active site and becomes motionally restricted, a process somewhat akin to the locking of a gate. Both the tight packing against the cofactor and the loss of flexibility in the loops undoubtedly help to retain the nicotinamide ring within its binding pocket in the active site in a geometry that is conducive to hydride transfer.

Together, the crystallographic, kinetic, and NMR data provide convincing evidence that the Met20 loop plays an important role in DHFR catalysis, acting as a gate that controls access of the nicotinamide ring of the cofactor to its binding pocket and that seals the active site in the Michaelis complex. The conformation of the loop, i.e., whether it is closed or it is occluded, appears to be determined largely by the occupancy of the nicotinamide binding pocket. This in turn is dependent upon the degree of steric clash between the nicotinamide and the pterin rings; there is overlap between the binding pockets for these rings such that the occupancy of the nicotinamide site is influenced by the extent of ring puckering (*10*).

Partial deletion of the Met20 loop does not affect the Michaelis parameters for binding of dihydrofolate or NADPH nor the off rate from the E:THF:$NADP^+$ complex (*18*). The rate of hydride transfer, however, is dramatically slowed from 950 to 1.7 s^{-1}. The inability of the mutant enzyme to seal the active site may result in a markedly reduced population of NAC conformations or uncouple motions from distal sites in the protein that affect the height of the energy barrier for the hydride transfer step. Indeed, mutations at G121 in the F−G loop (*19*) or at S148 in the G−H loop (*51*) act either to significantly slow the hydride transfer step by factors of up to 10^3 (F−G loop) or to modulate the ligand off rates by enhancing the affinity for $NADP^+$ and decreasing that for THF (G−H loop). The coupling of the Met20, F−G, and G−H loops is manifest in the changes observed in τ_e and R_{ex} terms for residues within these loop regions for the various complexes of DHFR involved in the turnover cycle. Although the Met20 loop appears to play an important function as a flexible gate controlling access to the active site, its movement cannot be rate limiting in the wild-type enzyme because a normal kinetic isotope effect associated with the hydride transfer step is observed in the steady-state kinetics at pH values where product release is fast (*17*). Moreover, a conformational change associated with gating, occurring prior to the chemical step, cannot be detected by stopped flow methods, indicating that it must occur at a rate faster than 2000 s^{-1} for the wild-type protein (*19*). However, for the G121V mutant, gating becomes kinetically significant because its rate is only 3-fold faster than that of the hydride transfer step as detected by pre-steady-state kinetics.

NMR studies have shown that motions are often prevalent at protein sites implicated in function. The importance of motions on similar time scales to the rate of a functional process is intuitive. Accordingly, a number of studies have shown the importance of millisecond/microsecond motions, particularly for signaling proteins (*52*−*54*). Conformational fluctuations of flexible loops are likely to be of importance for the function of many enzymes. Models for enzyme catalysis incorporating dynamics suggest that motions need to be as fast, or faster, than the rate of reaction (*1*, *13*, *55*). It is therefore interesting to see that motions on both fast and slow time scales, and significantly nanosecond motions for the Met20 loop, are important for DHFR function. In addition to DHFR, loop motions on both the picosecond/nanosecond and the microsecond time scales have been detected in HIV protease using ^{15}N relaxation measurements (*7*, *56*). These motions are localized to the flaps that cover the active site of the protease, and it has been suggested that they facilitate substrate access and product release (*7*). A flexible flap that closes over the active site in the presence of substrate has also been identified in the metallo-β-lactamase from *Bacteroides fragilis* (*57*). The motions of this flap can explain the broad catalytic scope of the enzyme, i.e., its ability to hydrolyze a broad range of substrates and also its catalytic efficiency. Finally, ^2H NMR measurements have shown that a flexible loop that covers the active site of triosephosphate isomerase fluctuates between open and closed states at a rate that is very similar to the catalytic turnover rate (*4*). With increasing interest in the use of NMR to study protein dynamics, many more enzymes will un-

doubtedly be added to this list, leading to a deeper understanding of the role of both backbone and side chain motions in biological catalysis.

ACKNOWLEDGMENT

We thank John Chung and Gerard Kroon for helpful discussions on the NMR experiments; Leiming Zhu for help with the implementation of the program SPIRIT; Ishwar Radhakrishnan, David Epstein, Eduardo Zaborowski, Brendan Duggan, Rani Venkitakrishnan, and James Huntley for helpful discussions; and Linda Tennant for expert technical assistance.

REFERENCES

1. Cannon, W. R., Singleton, S. F., and Benkovic, S. J. (1996) *Nat. Struct. Biol. 3*, 821−833.
2. Bruice, T. C., and Benkovic, S. J. (2000) *Biochemistry 39*, 6267−6274.
3. Cannon, W. R., and Benkovic, S. J. (1998) *J. Biol. Chem. 273*, 26257−26260.
4. Williams, J. C., and McDermott, A. E. (1995) *Biochemistry 34*, 8309−8319.
5. Epstein, D. M., Benkovic, S. J., and Wright, P. E. (1995) *Biochemistry 34*, 11037−11048.
6. Falzone, C. J., Wright, P. E., and Benkovic, S. J. (1994) *Biochemistry 33*, 439−442.
7. Nicholson, L. K., Yamazaki, T., Torchia, D. A., Grzesiek, S., Bax, A., Stahl, S. J., Kaufman, J. D., Wingfield, P. T., Lam, P. Y. S., Jadhav, P. K., Hodge, C. N., Domaille, P. J., and Chang, C.-H. (1995) *Nat. Struct. Biol. 2*, 274−280.
8. Lolis, E., and Petsko, G. A. (1990) *Biochemistry 29*, 6619−6625.
9. Rader, S. D., and Agard, D. A. (1997) *Protein Sci. 6*, 1375−1386.
10. Sawaya, M. R., and Kraut, J. (1997) *Biochemistry 36*, 586−603.
11. Young, L., and Post, C. B. (1996) *Biochemistry 35*, 15129−15133.
12. Cannon, W. R., Garrison, B. J., and Benkovic, S. J. (1997) *J. Am. Chem. Soc. 119*, 2386-2395.
13. Zhou, H. X., Wlodek, S. T., and McCammon, J. A. (1998) *Proc. Natl. Acad. Sci. U.S.A. 95*, 9280−9283.
14. Karplus, M., and McCammon, J. A. (1983) *Annu. Rev. Biochem. 53*, 263−300.
15. Kurzynski, M. (1997) *Biophys. Chem. 65*, 1−28.
16. Lau, E. Y., and Bruice, T. C. (1999) *Biophys. J. 77*, 85−98.
17. Fierke, C. A., Johnson, K. A., and Benkovic, S. J. (1987) *Biochemistry 26*, 4085−4092.
18. Li, L., Falzone, C. J., Wright, P. E., and Benkovic, S. J. (1992) *Biochemistry 31*, 7826−7833.
19. Cameron, C. E., and Benkovic, S. J. (1997) *Biochemistry 36*, 15792−15800.
20. Miller, G. P., and Benkovic, S. J. (1998) *Biochemistry 37*, 6336−6342.
21. Miller, G. P., and Benkovic, S. J. (1998) *Biochemistry 37*, 6327−6335.
22. Radkiewicz, J. L., and Brooks, C. L., III (2000) *J. Am. Chem. Soc. 122*, 225−231.
23. Osborne, M. J., and Wright, P. E. (2001) *J. Biomol. NMR 19*, 209−230.
24. Falzone, C. J., Cavanagh, J., Cowart, M., Palmer, A. G., III, Matthews, C. R., Benkovic, S. J., and Wright, P. E. (1994) *J. Biomol. NMR 4*, 349−366.
25. Lee, W., Revington, M. J., Arrowsmith, C., and Kay, L. E. (1994) *FEBS Lett. 350*, 87−90.
26. Farrow, N. A., Zhang, O., Szabo, A., Torchia, D. A., and Kay, L. E. (1995) *J. Biomol. NMR 6*, 153−162.
27. Palmer, A. G., Skelton, N. J., Chazin, W. J., Wright, P. E., and Rance, M. (1992) *Mol. Phys. 75*, 699−711.
28. Live, D. H., Davis, D. G., Agosta, W. C., and Cowburn, D. (1984) *J. Am. Chem. Soc. 106*, 6104−6105.
29. Bax, A., and Subramanian, S. (1986) *J. Magn. Reson. 67*, 565−569.
30. Zhu, G., Torchia, D. A., and Bax, A. (1993) *J. Magn. Reson. Ser. A 105*, 219−222.
31. Delaglio, F., Grzesiek, S., Vuister, G. W., Guang, Z., Pfeifer, J., and Bax, A. (1995) *J. Biomol. NMR 6*, 277−293.
32. Johnson, B. A., and Blevins, R. A. (1994) *J. Chem. Phys. 29*, 1012−1014.
33. Marion, D., Ikura, M., and Bax, A. (1989) *J. Magn. Reson. 84*, 425−430.
34. Palmer, A. G., Rance, M., and Wright, P. E. (1991) *J. Am. Chem. Soc. 113*, 4371−4380.
35. Stone, M. J., Fairbrother, W. J., Palmer, A. G., III, Reizer, J., Saier, M. H., Jr., and Wright, P. E. (1992) *Biochemistry 31*, 4394−4406.
36. Abragam, A. (1961) *Principles of Nuclear Magnetism*, Clarendon Press, Oxford.
37. Tjandra, N., Szabo, A., and Bax, A. (1996) *J. Am. Chem. Soc. 118*, 6986−6991.
38. Lee, L. K., Rance, M., Chazin, W. J., and Palmer, A. G. (1997) *J. Biomol. NMR 9*, 287−298.
39. Brüschweiler, R., Liao, X., and Wright, P. E. (1995) *Science 268*, 886−889.
40. Kroenke, C. D., Loria, J. P., Lee, L. P., Rance, M., and Palmer, A. G., III (1998) *J. Am. Chem. Soc. 120*, 7905−7915.
41. Clore, G. M., Szabo, A., Bax, A., Kay, L. E., Driscoll, P. C., and Gronenborn, A. M. (1990) *J. Am. Chem. Soc. 112*, 4989−4991.
42. Mandel, A. M., Akke, M., and Palmer, A. G., III (1996) *Biochemistry 35*, 16009−16023.
43. Zhu, L., Dyson, H. J., and Wright, P. E. (1998) *J. Biomol. NMR 11*, 17−29.
44. Wei, A., Raymond, M. K., and Roberts, J. D. (1997) *J. Am. Chem. Soc. 119*, 2915−2920.
45. Lipari, G., and Szabo, A. (1982) *J. Am. Chem. Soc. 104*, 4546−4559.
46. Lipari, G., and Szabo, A. (1982) *J. Am. Chem. Soc. 104*, 4559−4570.
47. Bystroff, C., and Kraut, J. (1991) *Biochemistry 30*, 2227−2239.
48. Pan, H., Lee, J. C., and Hilser, V. J. (2000) *Proc. Natl. Acad. Sci. U.S.A. 97*, 12020−12025.
49. Miller, G. P. (1997) Ph.D. Thesis, The Pennsylvania State University, State College.
50. Ahrweiler, P., and Frieden, C. (1991) *Biochemistry 30*, 7801−7809.
51. Miller, G. P., Wahnon, D. C., and Benkovic, S. J. (2001) *Biochemistry 40*, 867−875.
52. Feher, V. A., and Cavanagh, J. (1999) *Nature 400*, 289−293.
53. Volkman, B. F., Lipson, D., Wemmer, D. E., and Kern, D. (2001) *Science 291*, 2429−2433.
54. Loh, A. P., Pawley, N., Nicholson, L. K., and Oswald, R. E. (2001) *Biochemistry 40*, 4590−4600.
55. Sutcliffe, M. J., and Scrutton, N. S. (2000) *Trends Biochem. Sci. 25*, 405−408.
56. Ishima, R., Freedberg, D. I., Wang, Y. X., Louis, J. M., and Torchia, D. A. (1999) *Struct. Fold. Des. 7*, 1047−1055.
57. Huntley, J. J. A., Scrofani, S. D. B., Osborne, M. J., Wright, P. E., and Dyson, H. J. (2000) *Biochemistry 39*, 13356−13364.
58. Nicholls, A., Sharp, K. A., and Honig, B. (1991) *Proteins 11*, 281−296.
59. Koradi, R., Billeter, M., and Wüthrich, K. (1996) *J. Mol. Graphics 14*, 51−55.

BI010621K